Numerical modeling of flow stress and grain evolution of an Mg AZ31B alloy based on hot compression tests

R. A. R. Giorjao[1,2], E.F. Monlevade[2], *J. Avila[3], A.P. Tschiptschin[2].

[1] Welding Engineering, The Ohio State University, 1248 Arthur E Adams Dr 43221, Columbus, OH, USA

[2] Metallurgical and Materials Engineering Department, University of São Paulo, Av. Prof. Mello Moraes 2463, 05508-030 São Paulo, SP, Brazil

[3] UNESP – São Paulo State University, Campus of São João da Boa Vista, Av. Profª Isette Corrêa Fontão, 505, Jardim das Flores, 13876-750 - São João da Boa Vista, SP, Brazil.

ABSTRACT

Magnesium alloys offer a wide range of applications in modern lightweight structures, although, the correct forming parameters need to be found to reach a good combination of fine microstructure and the required mechanical properties. Several discrete and statistical methods have been proposed to simulate the dynamic recrystallization process and adopted to study microstructural evolution. However, the materials parameters necessary to develop these models are not widely available. Hence, industrial evaluation of these parameters is complex, unpractical for several types of material and time consuming for daily industrial applications. In that way, the thermomechanical behavior and grain size evolution modeling of the AZ31 alloy is proposed using isothermal compression data. Parameters to calculate coupled stress-strain-temperature parameters, dynamic recrystallization, volume fraction, and grain size were obtained from the stress-strain curves. Then, the data was input in Deform-3D software to simulate the hot deformation process and verify with experimental data the consistency of the values obtained. Measured grains size agreed with the conducted modeling, showing the reliability of strain-stress and grain size data on predicting dynamic recrystallization phenomena.

KeyWords: AZ31B; isothermal compression; dynamic recrystallization; finite element modeling; Gleeble simulation

*Corresponding author: Julian Arnaldo Avila Diaz, julian.avila@unesp.br

1. INTRODUCTION

Magnesium alloys present excellent specific properties such as good processing with high productivity, low density with favorable mechanical properties and resource-efficient recycling [1]. The potential for cost-efficient industrial lightweight structures associated with magnesium materials support the industries of automobile and aerospace, to fulfill stringent energy and environmental efficiency guidelines [1].

Metallic alloys present a pronounced relationship between microstructure evolution and mechanical properties [2]. Likewise, in the hot forming process, three crucial metallurgical phenomena arise changing microstructure and mechanical properties of metallic materials. First work hardening strengthens due to dislocation movements and dislocation generation within the crystal structure. Secondly and finally, dynamic recovery and dynamic recrystallization act in deformed grains reducing their stored energy by the removal or rearrangement of defects in their crystal structure [2]. Hence, knowing how these alloys behave in hot forming conditions is paramount for their industrial processing and corresponding mechanical application.

The development of numerical simulations is critical to model the microstructural and mechanical evolutions; thus, allowing to predict the microstructural changes and mechanical properties upon different forming conditions. Several approaches have been proposed to simulate dynamic recrystallization (DRX) and adapted to study microstructural evolution, such as the Monte Carlo (MC) and the cellular automaton (CA) methods [3–5]. Both methods are also probabilistic, but CA is relatively flexible in simulating different physical systems and effective in the calculation [4]. The CA method is based on the relationship between the nucleation sites and the dislocation density distribution. Dislocation density plays a very significant role in nucleation and microstructural evolution of DRX during hot deformation [4]. However, the materials parameters necessary to develop these methods, for example, nucleation rate; critical dislocation density, grain boundary mobility, are not widely available. Hence, industrial evaluation of these parameters is complex, unpractical for several types of material and time consuming for daily industrial applications.

The stress-strain curves obtained in standard hot deformation tests (such as compression, torsion, and tension) show a close relationship with the grain structures at the given deformation conditions [2]. This information aided by numerical simulation can be used to select forming parameters, e.g., dynamic recrystallization (DRX) start can be identified from changes in the slope of the strain hardening rate versus flow stress curves [6]. The following approach is easily develop using few deformations and microstructural

observation tests, providing a complete mechanical behavior and microstructural model for the material.

Alternatively, the use of the minimum in the absolute value of the strain hardening slope can be calculated from strain hardening rate-flow stress curves [7]. Xu et al., [8] working with an AZ91D alloy proposed a kinetics model of DRX consistent with the experimental strain stress data. Quan et al., [9] indicates whether DRX evolution can be characterized by the process variables from the conventional strain hardening rate curves. Liu et al., [10] analyzing AZ31B allow revealed that a kinetics model of DRX based on the strain-stress curves of compression tests were in good agreement with microscopic observation.

In the present work, stress-strain data from compressions tests and grain size analysis were used to model the thermomechanical behavior and grain size evolution of AZ31B alloy. The parameters found were applied in finite element software DEFORM-3D to simulate the hot deformation process. The results were used to compare and verify the consistency of the values obtained with experimental data. The results aim to provide relevant guidelines to hot deformation modeling techniques in the AZ31B alloy, depicting steps to develop the model for other metallic materials.

2. MATERIALS AND METHODS

Hot rolled 5-mm thick sheets of an AZ31B magnesium alloy with the chemical composition shown in

Table 1 were used in this study. Experimental data for the thermomechanical response, dynamic recrystallization and grain size evolution were obtained from strain-stress curves and microstructural analysis.

Table 1: Chemical composition of AZ31B magnesium alloy (%wt)

Element	Mg	Al	Si	Fe	Mn	Zn	P
AZ31B	Bal.	3.33	0.019	0.009	0.63	0.56	0.005

The isothermal hot compression tests were conducted in cylindrical samples with 5-mm diameter and 7-mm length. The tests were carried out at temperatures of 200 °C, 300 °C, 350 °C, 400 °C, 450 °C and 500 °C, and strain rates of 0.01 s^{-1}, 0.1 s^{-1}, 1 s^{-1} and 10 s^{-1}. Prior testing, a nickel-based lubricant was applied to the specimen end faces

to minimize the effects of friction on the contact surfaces. Specimens were first heated to the deformation temperature and held isothermally for 10 seconds, before the straining stage. The specimens were then compressed to a true strain of 0.8 using a Gleeble 3800 thermomechanical simulator, equipped with electrical resistance grips. The temperature was controlled by resistive heating, using a k-type thermocouple. After the heating and deformation process, the samples were cooled with helium to preserve the grain structure.

Samples were cut and mounted for metallography analysis. Conventional grinding and polishing were applied in these samples, and Picral solution (5 g picric acid, 15 ml acetic acid, 10 ml water and 100 ml ethanol) was used to reveal the microstructure. Microstructures images were taken by optical microscopy. In all analyzed samples (as-rolled specimens), the deformation axis selected was parallel to the rolling direction.

To model the material behavior during hot deformation, the dependence of flow stress on temperature and strain rate was obtained. To date, several empirical equations have been proposed to establish the deformation activation energy and hot deformation behavior of alloys. The most frequently used one is the Arrhenius equation based on Sellars and McTegart [11] equations relating to the strain rate, flow stress, and temperature. The hyperbolic law in the Arrhenius type equation gives better approximations between strain, temperature and stress parameter. Thus, Arrhenius described in Equation 1 was applied to the model. Where Q is the activation energy (kJ/mol), which is an important physical parameter acting as an indicator of deformation in the plasticity deformation theory, A and α ($\alpha = \beta/n1$) [MPa^{-1}] are material constants, σ is the flow stress (MPa), n is the stress exponent; R is the universal gas constant and, T is the absolute temperature [K]. The constants values of the analyzed material will be obtained through the mathematical treatment of the strain curves obtained in the compression tests.

$\dot{\varepsilon} = A[\sinh(\alpha\sigma)]^n exp\left[\frac{-Q}{RT}\right]$	**Equation 1**

To verify and simulate all conditions present in hot deformation tests, DEFORM-3D was used to simulate the hot compression experiment. DEFORM-3D is a powerful process simulation system designed to analyze the three-dimensional (3D) flow of complex metal forming processes. The data obtained from the experimental testing, such as flow stress temperature-strain-rate relationship, DRX volume fraction and grain size was applied to the DEFORM 3D simulation.

The 3D finite element modeling was conducted considering a plastic behavior in the tested AZ31B, and a rigid material model for the dies. The original meshes of the specimens were divided into 15000 three-node triangular elements. Time stepping of 0.001 seconds was set during the calculations. The compression tests were modeled in the vacuum, so only radiation emissivity in the workpiece was applied.

3. RESULTS

3.1 STRESS-STRAIN CURVE

The typical true stress-strain curves were obtained through isothermal compression testing and four stages should be noted in the stress-strain graphs, as can be observed in Figure 1. First, critical stress indicates recrystallization start and recovery phenomena, softening the material. The flow stress increases sharply to a peak value, attributed to the increase in dislocation density, representing the maximum stress attained applied temperature and strain rate. Subsequently, the stress decreases with increasing strain, and dominance of dynamic softening during the deformation process is gradual, reaching the stage of maximum softening rate. The flow stress decreases gradually until the dynamic balance between the work hardening and the softening induced by DRX, exhibiting steady-state flow stress.

Flow stress curves of AZ31B magnesium alloy in this work, show the typical characteristic of dynamic recrystallization softening, including a single peak followed by a steady-state flow. It is also revealed that the peak stress, critical stress, and steady-state stress increase with decreasing temperature and increasing strain rate, indicating a sensitive temperature and the behavior of the strain rate and flow stress in the AZ31B alloy. AZ31B magnesium alloys reported by Spigarelli et al. [12] and Juan Liu, Cui, and Li [13] exhibited similar flow stress behavior. The data were not corrected for barreling.

At low temperatures, the samples showed low ductility and fracture at low deformation levels, as seen in 200 °C in Figure 1 (a), where the maximum deformations reached 30% and 40% for 1 and $10s^{-1}$. Zimina et al. [14] also observed similar behavior in tensile tests with AZ31 in which observed a decrease in ductility in tests bellow 250 °C. The results may be related to the activation of slip systems at temperatures below 200 °C. Twins are observed in samples tested at 200 °C showing the lack of slip systems in this temperature. For hot deformation processes modeling, the author suggests using data above 300 °C to achieve high levels of plasticity.

Padilha et al. [15] compared the opposite effect of the strain rate and deformation temperature, where the increase of the deformation rate is equal to the lowering of the temperature. This observation is explained by the ability of crystal defects to settle and rearrange during deformation. Higher deformation rates hinder or even inhibit this rearrangement, raising its yield stress along with the deformation.

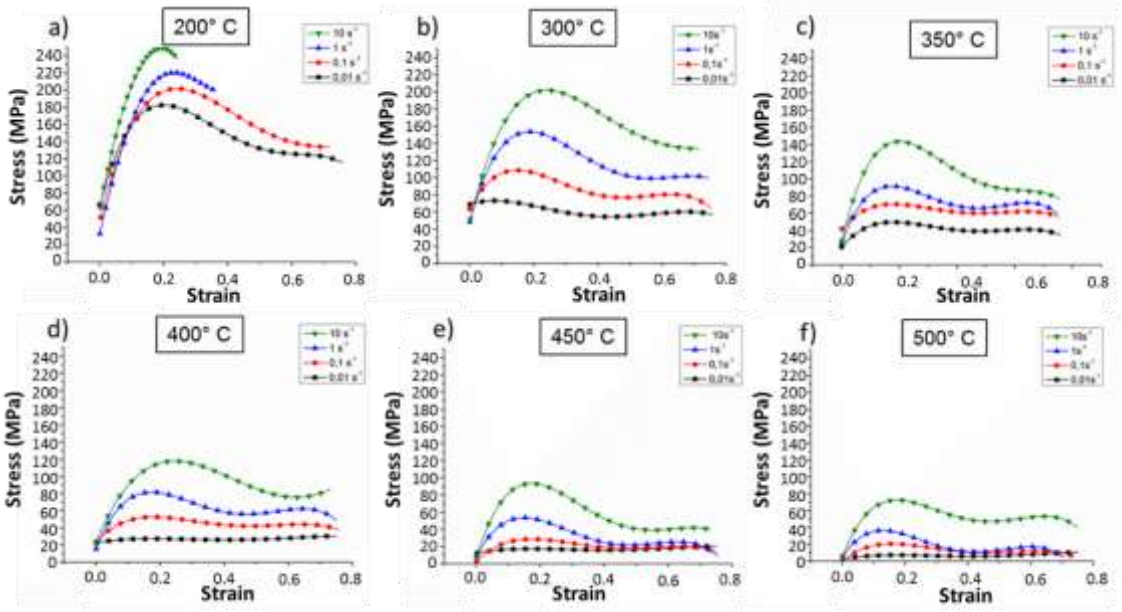

Figure 1: Isothermal stress-strain curves obtained by hot compression tests for different temperatures, (a) 200°C, (b) 300°C, (c) 350°C, (d) 400°C, (e) 450°C, (f) 500°C, and strain rates, 0.01 s^{-1}, 0.1 s^{-1}, 1 s^{-1} and 10 s^{-1}

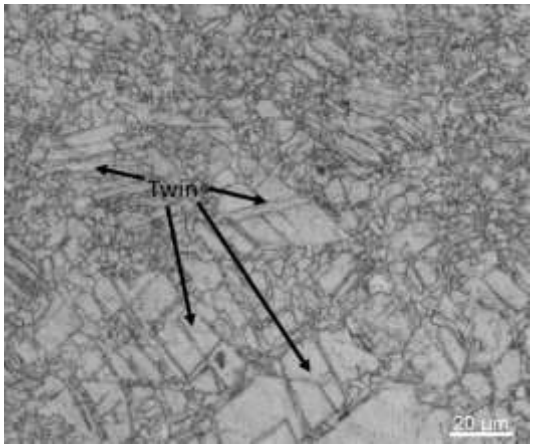

Figure 2: Twins observed in samples tested at 200 °C and 10 s^{-1}

3.2 CONSTITUTIVE ANALYSIS

Using Equation 1 and applying an *ln* logarithm, Equation 2 is obtained, where $\beta = d\ln\dot{\varepsilon}/d|\sigma|$. Thus, data can be approximated to a straight line, as shown in Figure 3. Equation 3 is slightly different from Equation 2, including the $n_1 = d\ln\dot{\varepsilon}/d\ln|\sigma|$. Therefore, the average of the slopes of lines in Figure 3 (a) is accepted as the constant material n. Thus the *n* value was obtained as 5.34. The mean value of all slope rates in Figure 3 (b) is accepted as the material constant β, in which a value of 0.078 was found. Thus, we could obtain the value of $\alpha = \beta/n1$, where α was equal to 0.014 MPa^{-1}. The found values were similar to some in the literature [10,16,17] for processing AZ30 alloys.

$\ln\dot{\varepsilon} = \ln A + \beta\|\sigma\| - \frac{Q}{RT}$	**Equation 2**

$\ln\dot{\varepsilon} = \ln A + n_1\ln\|\sigma\| - \frac{Q}{RT}$	**Equation 3**

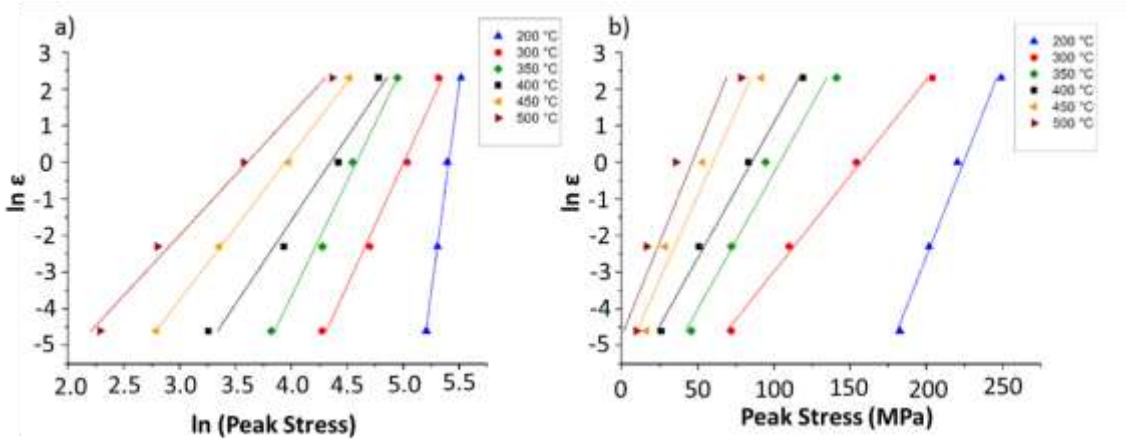

Figure 3: Relationship between ln ε and (a) ln σ_{peak} (b) σ_{peak}

For all the stress level, Eq. (1) can be rewritten as:

$\ln\dot{\varepsilon} = \ln[\sinh(\alpha\sigma)] + \ln A - \frac{Q}{R}\left(\frac{1}{T}\right)$	**Equation 4**

If $\dot{\varepsilon}$ is a constant, Eq (4) can be expressed as:

$Q = R\frac{\partial\ln\dot{\varepsilon}}{\partial\ln[\sinh(\alpha\sigma)]_T}\left\|\frac{\partial\ln[\sinh(\alpha\sigma)]}{\partial(1/T)}\right\|_{\dot{\varepsilon}}$	**Equation 5**

The linear relationships of $\ln \dot{\varepsilon}$ - $\ln[\sinh(\alpha\sigma)]$ and $\ln[\sinh(\alpha\sigma)]$ - $1/T$ at different strain rates were fitted as Figure 4. The mean value of all the slopes in Figure 4 (a) is n, and the mean value of all the slopes in Figure 4 (b) is D. Then, $Q = RnD$, and Q average was calculated as 128 KJ/mol.

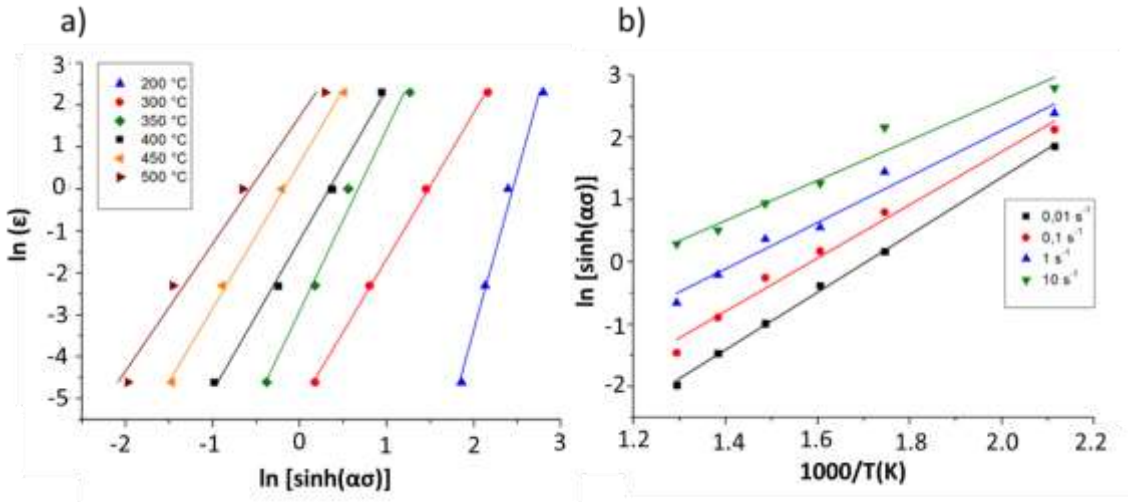

Figure 4: Relationship between $\ln[\sinh(\alpha\sigma)]$ and (a) $\ln \dot{\varepsilon}$ (b) 1/T

The last parameter $\boldsymbol{A}$ is found by replacing the values found in Equation 1, resulting in a value of 4.79 10^9 s^{-1}. The final equation is set in Equation 6.

$\dot{\varepsilon} = 4.79\ 10^9[\sinh(0.014\sigma)]^{3.88} exp\left[\frac{-128}{RT}\right]$	**Equation 6**

Table 2 summarizes the constants of the material studied and constants found in the literature for hot compression tests. The distinction between the material constants, which is not usually reported in papers, maybe due to variations in slip contact end-faces during compressions tests. For this reason, lubrication between the sample and the die leads to different responses of material plasticity.

Table 2: AZ31B hot deformation constants comparison

Parameters	n	Q (kJ/mol)
This Work	3.88	128
McQueen et al. [18]	1.8	130
Liao et al. [19]	5.23	145
Nourollahi et al. [20]	3.5	145
Bhattacharya et al. [21]	5.5	127

3.3 DYNAMIC RECRYSTALLIZED VOLUME FRACTION

DRX takes place at elevated temperatures, new grains evolve preferably in grain boundaries, advancing to prior grains interiors. Because of the low stacking fault energy of Mg alloy, the non-basal slip is hardly activated employing the broadly extended dislocation, which can cause DRX much more easily [22]. The DRX kinetics and grain size models can provide information on the DRX fraction and the DRX grain size [2].

Peak, critical and steady-state strain is important in determining DRX occurrence and is critical for the calculation of the recrystallization volume fraction. Microstructure observations usually are employed for determining the critical strain, however, it requires many samples to be examined. In this work, work hardening true stress-strain curves have been applied to track dynamic recrystallization critical stages and the dynamically recrystallized volume fraction. The strain hardening rate (θ) is defined by the derived stress concerning strain (dσ/dε). According to Padilha et al., [15] and Shaban et al., [23] work-hardening curves show typically four stages: stage I begins from initial stress to the critical stress (σ_c), where the value of θ decreases sharply, and the inflection point on the θ-σ curve demonstrates the onset of DRX. Stage II indicates the transition between the DRX start (corresponding to σ_c) to the peak stress, where θ decreases to zero. Stage III begins at σ_p and ends in σ^* where θ reaches the lowest value indicating the maximum softening region, where DRX is the predominant evolution mechanism. The steady-state stress (θ=0) in stage IV indicates the equilibrium between work hardening and DRX softening. Using Figure 5 and Figure 1 data, e.g., peak stress (σ_p), critical stress (σ_c), maximum softening stress (σ^*), steady-state stress (σ_{ss}), peak strain (ε_p), critical strain (ε_c), maximum softening strain (ε^*) and steady-state strain (ε_{ss}), hardening rate ($\theta=d\sigma/d\varepsilon$) versus flow stress (σ) curves were obtained for all analyzed conditions, as depicted in Figure 5.

The relationship between the critical stress and the peak stress calculated in this work was 0.33. The values of this relationship were also reported by other authors: Xu et al. [8] reported values of 0.212 to 0.666 for alloy AZ91D, Quan et al. [24] found values of 0.270-0.522 for AZ80 alloy and Liu et al. [10] determined the value of 0.81 for AZ31 alloy. The relationship between critical strain and peak strain obtained in the present study presents an average lower than the value of 0.81 adopted by Liu et al., [10]. It should be noted that the verification of critical strain values presents uncertainties that may result in observed differences, as discussed by Liu et al. [10].

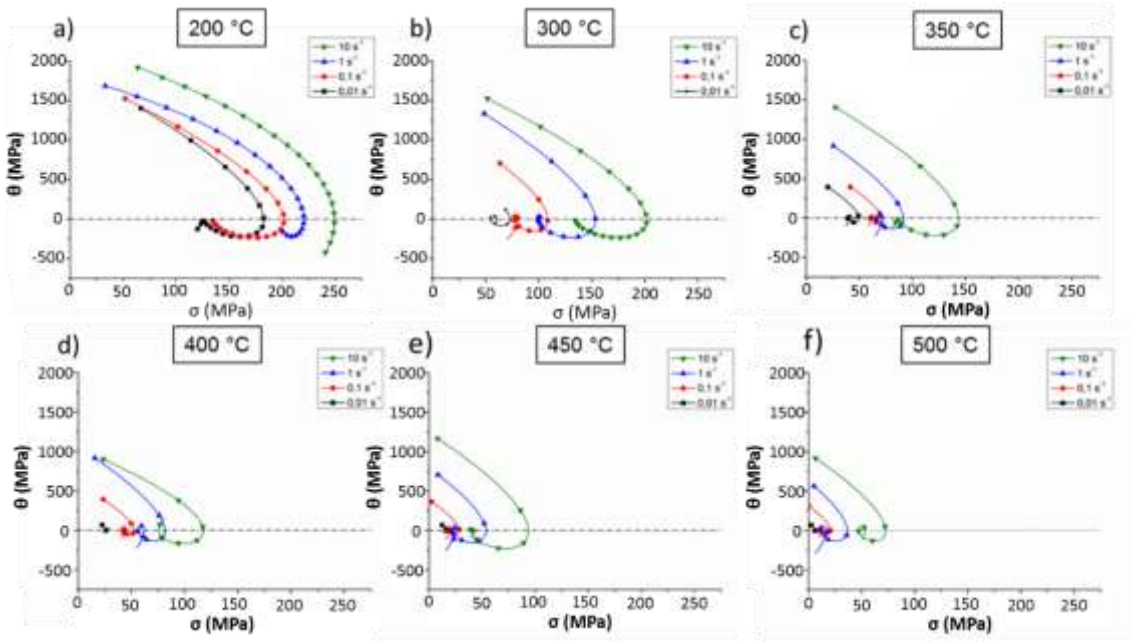

Figure 5: Hardening rate (θ=dσ/dε) curves of the experimental alloy obtained by hot compression tests. Test performed from 200°C to 500°C and from 0.01s^{-1} to 10s^{-1} strain rate

The Zener-Hollomon parameter (Z) - Equation 7- presents the combined influences of temperature and strain rate in an exponential equation. In this way, it allows its application in mathematical models of phenomena that consider the effects of temperature and deformation.

$Z = \dot{\varepsilon} \cdot \exp\left(\frac{Q}{RT}\right)$	**Equation 7**

According to Sellars et al. [25] and Mcqueen et al. [26], strain, stress, and recrystallized grain size can be written as a function of the Zenner-Hollomon parameter. Thus, peak deformation, deformation to 50% recrystallized fraction and recrystallized grain size were expressed using the dimensionless relationship (Z/A), as seen in

Equation 8, Equation 9, and Equation 10. This type of approach was also applied by Quan et al. [24], Bin-Jiang et al. [27] and Xu et al. [8] in studies of magnesium alloys.

$\varepsilon_p = C_1 \cdot \left(\frac{Z}{A}\right)^{m1}$	**Equation 8**

$\varepsilon_{0.5} = C_2 \cdot \left(\frac{Z}{A}\right)^{m2}$	**Equation 9**

$d_{DRX} = C_3 \cdot \left(\frac{Z}{A}\right)^{m3}$	**Equation 10**

The parameter A, as previously mentioned, is a constant of the analyzed material. The value of ε_p was modeled as a function of strain rate and temperature, as depicted in Equation 11, where ε_p denotes the strain corresponding to the flow stress maximum; a_1 is the material constant; m_1 is the strain-rate exponent. To obtain the parameters, the logarithmic relationship between ε_p e $\left(\frac{Z}{A}\right)$, was established. Hence, after fitting the data, a_1, m_1, and Q_1 are known, the peak strain ε_p may be calculated from Equation 12 for different strain rates and temperatures.

$\varepsilon_p = a_1 \cdot \dot{\varepsilon}^{m_1} \cdot \exp\left(\frac{Q_1}{RT}\right)$	**Equation 11**

$\varepsilon_p = 0.0771 \cdot \dot{\varepsilon}^{0.031} \cdot \exp\left(\frac{3968}{RT}\right)$	**Equation 12**

3.4 RECRYSTALLIZED VOLUME FRACTION

The evolution of microstructure due to DRX can be predicted by the modified Avrami type equation, as shown by Liu et al.,[10] and others [16,28]. The fraction of recrystallized DRX however, at a constant strain rate, time can be replaced by strain, as seen in Equation 13 where, a_{10}, β_d, and k_d are the material constants.

$X_{DRX} = 1 - exp\left[-\beta_d \left(\frac{\varepsilon - a_{10}\varepsilon_p}{\varepsilon_{0.5}}\right)^{k_d}\right]$	**Equation 13**

To solve the material constant β_d and k_d, it is essential to identify the deformation conditions corresponding to X_{DRX}=1, which suggests the flow stress at a steady-state and complete DRX grains in equiaxed shape and constant size. Then, an additional equation was used, as shown in Equation 14. According to Bergstrom [29], the recrystallized fraction of metal can be described as a relation between the stress of the material in a considered strain, peak stress, and steady-state stress. Thus, the volume fraction of DRX was plotted in Figure 6 using Equation 14 and the true stress-strain data. The S-shape curves of DRX showed a direct increase of DRX fraction in the microstructure with temperature and inversely with strain rate. High temperatures support the acceleration of DRX activation mechanisms while high strain rates give less time to nucleation and growth by DRX.

$X_{DRX} = \frac{\sigma - \sigma_p}{\sigma_s - \sigma_p}$	**Equation 14**

For a stated temperature in Figure 6, e.g., 450 °C, the 50% recrystallized volume fraction is reached later in faster strain rates, so DRX is delayed. A similar effect is noticed for the same strain rate, but in different temperatures, indicating a DRX delay in lower temperatures. Increasing strain rate and decreasing deformation temperature attend both, increases in dislocation density and reduction in the fraction of mobile dislocation.

Under 300 °C, the material did not reach 100% volume fraction DRX. This effect is attributed to decreased mobility of grain boundaries with increasing strain rate and decreasing temperature. Also, HCP crystal structure of Mg alloy lacks slip systems. Under a low deformation temperature, prism and pyramidal slip cannot be activated, resulting in a material with brittle characteristics. Hence, the corresponding recrystallization fraction curve for 200 °C was not shown. Due to the lack of data, the analysis under 300 °C was not included in the model.

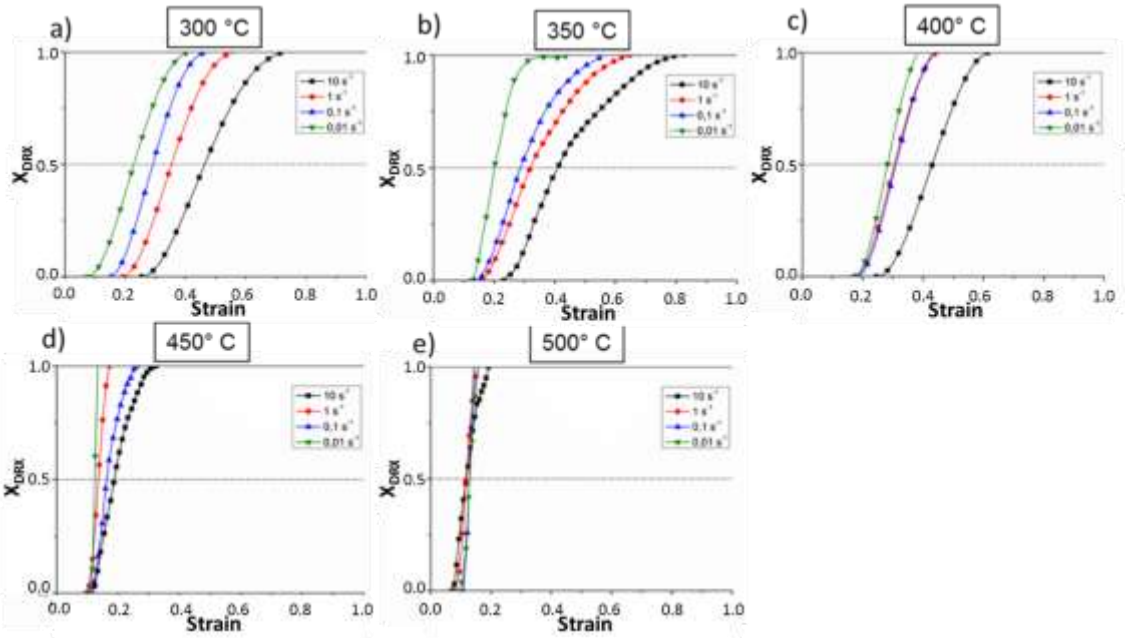

Figure 6: Volume fraction of DRX and strain rates

Therefore, using data from the recrystallized volume fraction and the true stress-strain data, the constants for Equation 14 was determined for the conditions analyzed in this paper, resulting in Equation 15. This equation can be used to determine the volume fraction of DRX in different strain conditions.

$X_{DRX} = 1 - exp\left[-0.639\left(\frac{\varepsilon - 0.005\varepsilon_p}{\varepsilon_{0.5}}\right)^{4.39}\right]$	**Equation 15**

Xu, Hu, and Sun [8] also found β_d and k_d with values of 0.677 and 2.86 respectively through regression analysis. The difference may be due to the small temperature range used in the tests (220 to 380 °C) fitting parameters for lower temperatures conditions, where higher deformation is required to achieve 100% DRX volume fraction.

The 50% DRX volume was calculated from the curves presented in the curves of Figure 6. The data was compiled in an Arrhenius type equation, as shown in Equation 16, where $\varepsilon_{0.5}$ denotes the strain for 50% recrystallization, a_5, $\dot{\varepsilon}$, m_2 and Q_2 are material constants. Likewise, to obtain the parameters, the logarithmic relationship between $\ln \varepsilon_{50\%}$ and $\ln\left(\frac{Z}{A}\right)$, then after fitting the data, the constants are known, the deformation

at 50% recrystallization can be calculated with Equation 17 as a function of strain rates and temperatures.

$\varepsilon_{0.5} = a_5 \cdot \dot{\varepsilon}^{m_2} \cdot \exp\left(\frac{Q_2}{RT}\right)$	**Equation 16**

$\varepsilon_{50\%} = 0.098 \cdot \dot{\varepsilon}^{0.036} \cdot \exp\left(\frac{4608}{RT}\right)$	**Equation 17**

3.5 DYNAMIC RECRYSTALLIZED GRAIN SIZE

Micrographs of the compressed specimens were used to determine the equation constants. Some examples of the microstructure of AZ31B compressed samples for 0.01 and 10 s^{-1} strain rates at different temperatures are shown in Figure 7. The microstructure of the compressed samples shows a tendency in both strain rates. For a fixed temperature, as strain rate increases, recrystallized grains have no enough growth time, and stored energy (i.e., high nucleation rate) increases, thus more refined grains will be achieved. Similar results were found by Guo-zheng et al., [31] processing 42CrMo Steel and Fatemi-Varzaneh et al., [32] processing AZ31 alloy.

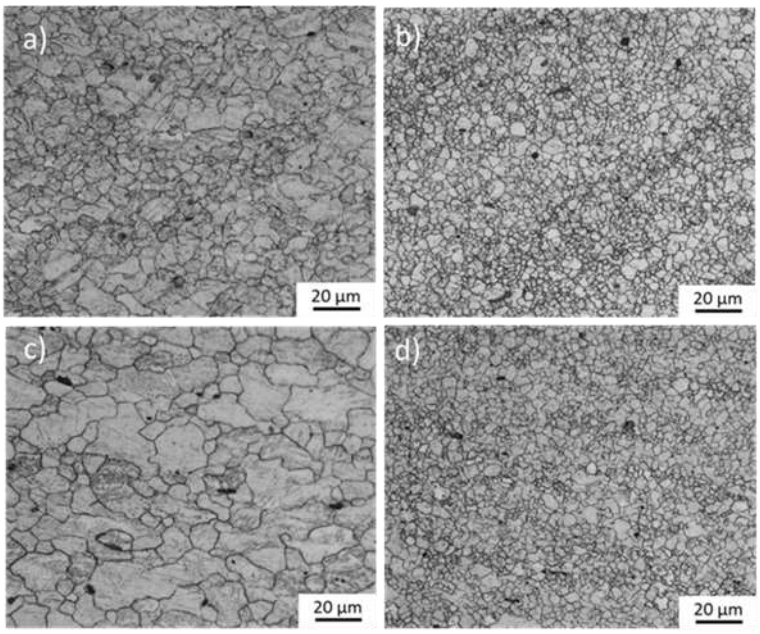

Figure 7: Examples of optical micrographs for (a) 0.01 s^{-1} at 400°C; (b) 10s^{-1} at 400°C; (c) 0.01 s^{-1} at 450°C and (d) 10s^{-1} at 450°C;

Grain size measurements were performed according to ASTM E112-12 [30]. Initial grains were still observable in the microstructure for lower temperatures. At the same temperature, smaller grain sizes were obtained at higher strain rates, as previously discussed. Grains with 1.85 µm were obtained for 300 °C/ 10s^{-1} conditions. Increasing temperature results in coarser DRX grains. The largest grains were obtained in the condition 500 °C/ 0.01 s^{-1}, with 24.07 µm. The grain size data was plotted evidencing the effect of temperature and strain rate, as depicted in Figure 8. According to the results, at high strain rates, the effect of temperature in grain size was less evident. For future studies, the author suggests evaluating different strain levels to increase model capabilities.

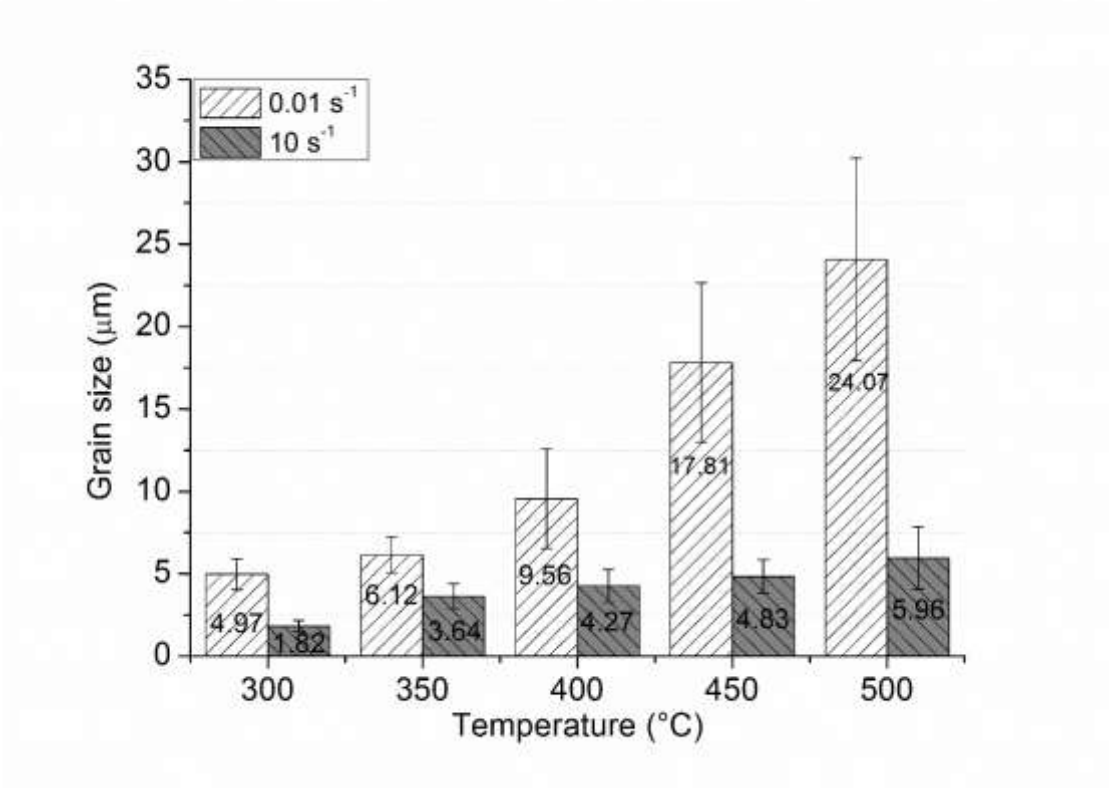

Figure 8: Grain size (µm) and standard deviation of the hot compressed specimens

The dynamic recrystallized grain size was calculated by an Arrhenius type equation, as seen in Equation 18.

$d_{DRX} = a_3 \cdot d_0^{n_3} \cdot \dot{\varepsilon}^{m_3} \cdot \exp\left(\frac{Q_3}{RT}\right)$	**Equation 18**

As previously applied, the constants of the recrystallized grain size equation were obtained by analyzing the logarithmic curves between $ln\, d_{DRX}$ e $ln\left(\frac{Z}{A}\right)$. Therefore, the diameter obtained by different strain rates and temperatures can be calculated by Equation 19.

$d_{DRX} = 473 \cdot \dot{\varepsilon}^{-0.2} \cdot \exp\left(\frac{-25539}{RT}\right)$	**Equation 19**

The activation energy for the DRX grain size obtained differs from Lee et al. [33] which found the value of 17860 J. The variation might be due to the author used only one temperature (300 °C) to formulate the grain size equation.

The constitutive equation, DRX volume fraction, and DRX grain size equation were applied in hot compression simulation in DEFORM 3D software. The friction coefficient between die and billet was adjusted to fit simulated with the experimental force curves resulting in a value of 0.3. Examples of the adjusted force curves can be seen in Figure 9

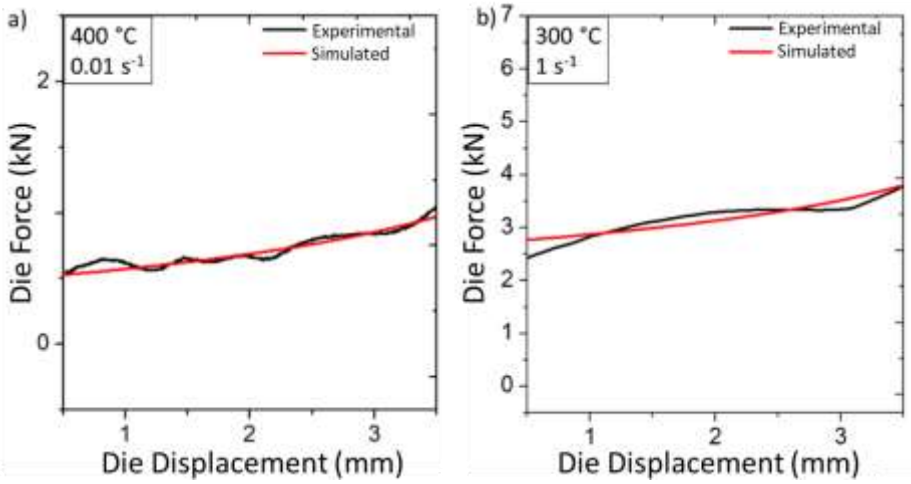

Figure 9: Die force and dislocation comparison between experimental and simulated results for the conditions (a) 400 °C, 0.01 s^{-1} e (b) 300 °C, 10 s^{-1}

After simulation completed for all temperatures, the grain size in the cross-section was analyzed. Two examples can be seen in Figure 10. For the model validation, two strain rates were used, and the final grain size values were compared with experimental

values, as seen in Figure 10 (b). The simulation results showed a great agreement with the experimental data. Hence, this modeling offers a new approach to predict grain features from simple strain-stress curves and microstructural observation, which are easy to be conducted in basic industrial research labs. Former approaches do require complex parameters to be determined before modeling, e.g., nucleation rate; critical dislocation density and grain boundary mobility for the CA method [4]. Also, this modeling can be applied independently of the geometrical aspects of the experimental sample.

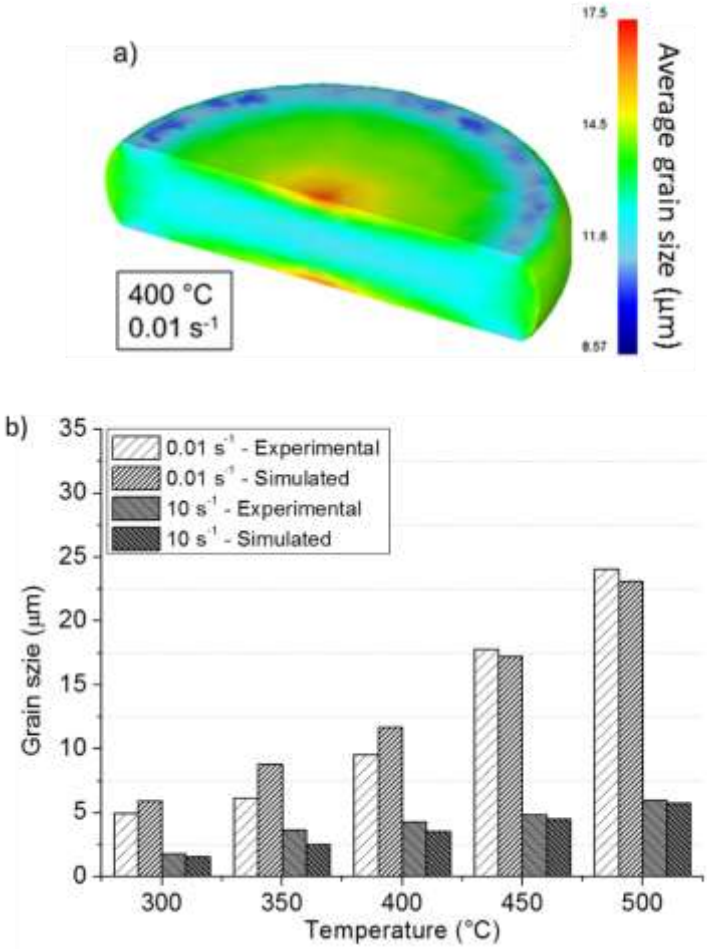

Figure 10: Transverse section of the simulated compression test specimens for the conditions of (a) 400 ° C, 0.01 s^{-1} and (b) grain size comparison between experimental and simulated approaches

4. CONCLUSIONS

- The present results demonstrate the robustness of the modeling method for microstructural and mechanical evaluation using hot compression data and microstructural observations, widely available in laboratories and research centers in metal materials.

- Flow stress curves of AZ31B magnesium alloy in this work shows clear features of dynamic recrystallization softening, including a single peak followed by a steady-state flow, which is affected by temperature and strain rate.
- The activation energy determined in the present study, 128 kJ/mol, calculated using hyperbolic law in the Arrhenius type equation. This result agrees with the reported in the literature, suggesting that dynamic recrystallization is the main softening mechanism for the hot deformation of AZ31B. The distinction between the material constants between authors may be due to variations in slip contact end-faces during compressions tests.
- During compression assessment, the elevated temperatures provide conditions for dynamic recrystallization, promoting grain refinement. For slower strain rates, the energy applied in the sample turn increasing the new grains nucleated, providing larger grain sizes as the temperature increases.
- The simulation results showed a great agreement with the experimental data. Microstructure observation shows that the proposed kinetics and grain size model of DRX is consistent with the experimental data.
- Some important parameters such as the activation energy of DRX (Q), the critical strain for DRX initiation (ε_c), the strain for peak stress (ε_p), and the strain for maximum softening rate (ε^*) were determined through this research.

Acknowledgments

The authors thank LNNano and Villares Metals for technical support.

References

[1] D.S. Kumar, C.T. Sasanka, K. Ravindra, K.N.S. Suman, Magnesium and Its Alloys in Automotive Applications – A Review, Am. J. Mater. Sci. Technol. (2015). https://doi.org/10.7726/ajmst.2015.1002.

[2] F.J. Humphreys, M. Hatherly, Hot Deformation and Dynamic Restoration, in: Recryst. Relat. Annealing Phenom., 2° Edition, Elsevier, 2004: pp. 415–V. https://doi.org/10.1016/B978-008044164-1/50017-7.

[3] Y. He, H. Ding, L. Liu, K. Shin, Computer simulation of 2D grain growth using a cellular automata model based on the lowest energy principle, Mater. Sci. Eng. A. 429 (2006) 236–246. https://doi.org/10.1016/j.msea.2006.05.070.

[4] X. LIU, L. LI, F. HE, J. ZHOU, B. ZHU, L. ZHANG, Simulation on dynamic recrystallization behavior of AZ31 magnesium alloy using cellular automaton method coupling Laasraoui–Jonas model, Trans. Nonferrous Met. Soc. China. 23 (2013) 2692–2699. https://doi.org/10.1016/S1003-6326(13)62786-7.

[5] S.H. Choi, D.W. Kim, B.S. Seong, A.D. Rollett, 3-D simulation of spatial stress distribution in an AZ31 Mg alloy sheet under in-plane compression, Int. J. Plast. 27 (2011) 1702–1720. https://doi.org/10.1016/j.ijplas.2011.05.014.

[6] N.D. Ryan, H.J. McQueen, Dynamic Softening Mechanisms in 304 Austenitic Stainless Steel, Can. Metall. Q. 29 (1990) 147–162. https://doi.org/10.1179/cmq.1990.29.2.147.

[7] E.I. Poliak, J.J. Jonas, A one-parameter approach to determining the critical conditions for the initiation of dynamic recrystallization, Acta Mater. 44 (1996) 127–136. https://doi.org/10.1016/1359-6454(95)00146-7.

[8] Y. Xu, L.X. Hu, Y. Sun, Dynamic recrystallization kinetics of as-cast AZ91D alloy, Trans. Nonferrous Met. Soc. China (English Ed. 24 (2014) 1683–1689. https://doi.org/10.1016/S1003-6326(14)63241-6.

[9] G.Z. Quan, Y.P. Mao, G.S. Li, W.Q. Lv, Y. Wang, J. Zhou, A characterization for the dynamic recrystallization kinetics of as-extruded 7075 aluminum alloy based on true stress-strain curves, Comput. Mater. Sci. 55 (2012) 65–72. https://doi.org/10.1016/j.commatsci.2011.11.031.

[10] J. Liu, Z. Cui, L. Ruan, A new kinetics model of dynamic recrystallization for magnesium alloy AZ31B, Mater. Sci. Eng. A. 529 (2011) 300–310. https://doi.org/10.1016/j.msea.2011.09.032.

[11] C.M. Sellars, W.J. McTegart, On the mechanism of hot deformation, Acta Metall. 14 (1966) 1136–1138. https://doi.org/10.1016/0001-6160(66)90207-0.

[12] S. Spigarelli, M. El Mehtedi, M. Cabibbo, E. Evangelista, J. Kaneko, A. Jäger, V. Gartnerova, Analysis of high-temperature deformation and microstructure of an AZ31 magnesium alloy, Mater. Sci. Eng. A. 462 (2007) 197–201. https://doi.org/10.1016/j.msea.2006.03.155.

[13] J. Liu, Z. Cui, C. Li, Modelling of flow stress characterizing dynamic recrystallization for magnesium alloy AZ31B, Comput. Mater. Sci. 41 (2008) 375–382. https://doi.org/10.1016/j.commatsci.2007.04.024.

[14] M. Zimina, P. Málek, J. Bohlen, D. Letzig, G. Kurz, M. Cieslar, Mechanical

properties of homogenized twin-roll cast and conventionally cast AZ31 magnesium alloys, Mater. Eng. 22 (2015) 8–15.

[15] F. PADILHA, A. F., SICILIANO Jr., Encruamento, recristalização, crescimento de grão e textura, ABM, São Paulo, 2005.

[16] Y. Xu, L. Hu, Y. Sun, Deformation behaviour and dynamic recrystallization of AZ61 magnesium alloy, J. Alloys Compd. 580 (2013) 262–269. https://doi.org/10.1016/j.jallcom.2013.05.082.

[17] S. Aliakbari Sani, G.R. Ebrahimi, A.R. Kiani Rashid, Hot deformation behavior and dynamic recrystallization kinetics of AZ61 and AZ61 + Sr magnesium alloys, J. Magnes. Alloy. 4 (2016) 104–114. https://doi.org/10.1016/j.jma.2016.05.001.

[18] H.J. McQueen, M. Myshlaev, M. Sauerborn, A. Mwembela, FLOW STRESS MICROSTRUCTURES AND MODELING IN IN HOT EXTRUSION OF MAGNESIUM ALLOYS, Miner. Met. Mater. Soc. (2000) 1–8.

[19] C. Liao, H. Wu, C. Wu, F. Zhu, S. Lee, Hot deformation behavior and flow stress modeling of annealed AZ61 Mg alloys, Prog. Nat. Sci. Mater. Int. 24 (2014) 253–265. https://doi.org/10.1016/j.pnsc.2014.04.006.

[20] G.A. Nourollahi, M. Farahani, A. Babakhani, S.S. Mirjavadi, Compressive deformation behavior modeling of AZ31 magnesium alloy at elevated temperature considering the strain effect, Mater. Res. 16 (2013) 1309–1314. https://doi.org/10.1590/S1516-14392013005000149.

[21] R. Bhattacharya, Y.J. Lan, B.P. Wynne, B. Davis, W.M. Rainforth, Constitutive equations of flow stress of magnesium AZ31 under dynamically recrystallizing conditions, J. Mater. Process. Technol. 214 (2014) 1408–1417. https://doi.org/10.1016/j.jmatprotec.2014.02.003.

[22] S.E. Ion, F.J. Humphreys, S.H. White, Dynamic recrystallisation and the development of microstructure during the high temperature deformation of magnesium, Acta Metall. 30 (1982) 1909–1919. https://doi.org/10.1016/0001-6160(82)90031-1.

[23] M. Shaban, B. Eghbali, Determination of critical conditions for dynamic recrystallization of a microalloyed steel, Mater. Sci. Eng. A. 527 (2010) 4320–4325. https://doi.org/10.1016/j.msea.2010.03.086.

[24] G.Z. Quan, Y. Shi, Y.X. Wang, B.S. Kang, T.W. Ku, W.J. Song, Constitutive modeling for the dynamic recrystallization evolution of AZ80 magnesium alloy

based on stress-strain data, Mater. Sci. Eng. A. 528 (2011) 8051–8059. https://doi.org/10.1016/j.msea.2011.07.064.

[25] C.M. Sellars, J. a. Whiteman, Recrystallization and grain growth in hot rolling, Met. Sci. 13 (1978) 187–194. https://doi.org/10.1179/msc.1979.13.3-4.187.

[26] H.J. Mcqueen, J.J. Jonas, Recent advances in hot working: Fundamental dynamic softening mechanisms, J. Appl. Metalwork. 3 (1984) 233–241. https://doi.org/10.1007/BF02833651.

[27] B.-J. Lv, J. Peng, D.-W. Shi, A.-T. Tang, F.-S. Pan, Constitutive modeling of dynamic recrystallization kinetics and processing maps of Mg–2.0Zn–0.3Zr alloy based on true stress–strain curves, Mater. Sci. Eng. A. 560 (2013) 727–733. https://doi.org/10.1016/j.msea.2012.10.025.

[28] Y. HE, Q. PAN, Q. CHEN, Z. ZHANG, X. LIU, W. LI, Modeling of strain hardening and dynamic recrystallization of ZK60 magnesium alloy during hot deformation, Trans. Nonferrous Met. Soc. China. 22 (2012) 246–254. https://doi.org/10.1016/S1003-6326(11)61167-9.

[29] Y. Bergström, A dislocation model for the stress-strain behaviour of polycrystalline α-Fe with special emphasis on the variation of the densities of mobile and immobile dislocations, Mater. Sci. Eng. 5 (1970) 193–200. https://doi.org/10.1016/0025-5416(70)90081-9.

[30] Astm Standard, E112-12:Standard Test Methods for Determining Average Grain Size, ASTM Int. E112-12 (2012) 1–27. https://doi.org/10.1520/E0112-12.1.4.

[31] Q. Guo-Zheng, W. Yang, L. Ying-Ying, Z. Jie, Effect of temperatures and strain rates on the average size of grains refined by dynamic recrystallization for as-extruded 42CrMo steel, Mater. Res. 16 (2013) 1092–1105. https://doi.org/10.1590/S1516-14392013005000091.

[32] S.M. Fatemi-Varzaneh, A. Zarei-Hanzaki, H. Beladi, Dynamic recrystallization in AZ31 magnesium alloy, Mater. Sci. Eng. A. 456 (2007) 52–57. https://doi.org/10.1016/j.msea.2006.11.095.

[33] B.H. Lee, N.S. Reddy, J.T. Yeom, C.S. Lee, Flow softening behavior during high temperature deformation of AZ31Mg alloy, J. Mater. Process. Technol. 187–188 (2007) 766–769. https://doi.org/10.1016/j.jmatprotec.2006.11.053.